JACS
JOURNAL OF THE AMERICAN CHEMICAL SOCIETY
Communication
pubs.acs.org/JACS

$RbMgCO_3F$: A New Beryllium-Free Deep-Ultraviolet Nonlinear Optical Material

T. Thao Tran,[†] Jiangang He,[§] James M. Rondinelli,*[,§] and P. Shiv Halasyamani*[,†]

[†]Department of Chemistry, University of Houston, Houston, Texas 77204-5003, United States
[§]Department of Materials Science and Engineering, Northwestern University, Evanston, Illinois 60208-3108, United States

Supporting Information

ABSTRACT: A new deep-ultraviolet nonlinear optical material, $RbMgCO_3F$, has been synthesized and characterized. The achiral nonpolar acentric material is second harmonic generation (SHG) active at both 1064 and 532 nm, with efficiencies of 160 × α-SiO_2 and 0.6 × β-BaB_2O_4, respectively, and exhibits a short UV cutoff, below 190 nm. $RbMgCO_3F$ possesses a three-dimensional structure of corner-shared $Mg(CO_3)_2F_2$ polyhedra. Unlike other acentric carbonate fluorides, in this example, the inclusion of Mg^{2+} creates pentagonal channels where the Rb^+ resides. Our electronic structure calculations reveal that the denticity of the carbonate linkage, monodentate or bidendate, to the divalent cation is a useful parameter for tuning the transparency window and achieving the sizable SHG response.

Materials capable of generating coherent deep-ultraviolet (DUV) light, λ < 200 nm, E_g > 6.2 eV, are of intense academic and technological interest attributable to their uses in photolithography, atto-second pulse generation, and advanced instrument development.[1,2] Generating coherent deep-UV light may be done through cascaded frequency conversion of nonlinear optical (NLO) materials, i.e., sixth harmonic generation of 1064 nm (Nd:YAG) radiation to 177.3 nm. From a crystal design and synthetic chemistry perspective, it is an ongoing challenge to discover a new material that is crystallographically non-centrosymmetric (NCS), exhibits a wide band gap (large transparency window), has a large second harmonic generation (SHG) coefficient with moderate birefringence, is chemically stable with a large laser damage threshold, and is easy to grow as large (cm^3) single crystals. Currently, only $KBe_2BO_3F_2$ (KBBF) is capable of generating coherent light below 200 nm using direct SHG methods.[3] With KBBF, single crystals tend to layer along their optical axis, thus hindering their practical applications.[4] Also, the need for highly toxic BeO in their synthesis and crystal growth complicates the detailed investigation of their properties. Thus, it is of great interest to discover DUV NLO materials that do not contain beryllium.

Other than KBBF, NCS borates are the most common materials for DUV NLO applications. LiB_3O_5 (LBO)[5] and CsB_3O_5 (CBO)[5,6] have absorption edges of 155 and 167 nm, respectively. The poor birefringence in both materials, 0.045 (LBO)[7] and 0.063 (CBO),[6] prevents them from being used for DUV NLO applications. β-BaB_2O_4 (β-BBO) has an appropriate birefringence, 0.1127;[8] however, its absorption edge of 185 nm[7] precludes the material from being used for sixth harmonic Nd:YAG generation. A number of other methods have been discussed for designing new NLO materials. These include using cations susceptible to second-order Jahn−Teller distortions,[9] cations with a stereo-active lone-pair,[10] and asymmetric chalcogenide polyhedra.[11] An issue with all of these design strategies is that the absorption edge is red-shifted. Thus, the materials are not suitable for DUV NLO applications.

Mixed-metal carbonate fluorides, which are accessible through hydrothermal synthesis, are a promising[12] materials family[13] for DUV NLO applications. They exhibit two unique attributes: (i) Fully bonded $(CO_3)^{2-}$ units, i.e., there is(are) no dangling O-atom(s). It has been shown in borates that the terminal O-atom red-shifts the absorption edge, making it difficult to reach the DUV.[14] (ii) The inclusion of fluoride also blue-shifts the absorption edge.[1f,4c] Thus, the materials are much more amenable to transmission in the DUV. Recently, two families of NCS carbonate fluorides have been reported, $ABCO_3F$ (A^+ = K, Rb, Cs; B^{2+} = Ca, Sr, Ba, and Pb)[15] and $Na_8Lu_2(CO_3)_6F_2$ and $Na_8Lu(CO_3)_2F_2$.[16] Although quantitative measurements of the optical gaps have yet to be determined, all materials are reported to have an absorption edge below 200 nm. Remarkably, the B = Mg member of this family has gone unreported, likely attributable to the low decomposition temperature of $MgCO_3$ compared with the other alkaline-earth carbonates.

Here we report the successful solid-state and hydrothermal synthesis of the achiral nonpolar NCS $RbMgCO_3F$ with an unusual pentagonal planar arrangement of $[Mg(CO_3)]_\infty$ owing to the A and B cation variance. It exhibits a powder SHG response at both 1064 and 532 nm incident radiation, with a short absorption edge, below 190 nm. Electronic structure calculations on $RbMgCO_3F$ reveal that, although the compound exhibits enhanced acentric displacements, which usually anti-correlate with the SHG response in these carbonate fluorides, this compound delivers an enhanced response owing to the non-uniform mono- and bidentate ligand bonding of Mg^{2+}. The results indicate $RbMgCO_3F$ could be an excellent candidate for optical technologies operating in the DUV utilizing nonlinear light−matter interactions.

$RbMgCO_3F$ crystallizes in the achiral nonpolar space group $P\bar{6}2m$ and exhibits a three-dimensional crystal structure consisting of corner-sharing $Mg(CO_3)_3F_2$ polyhedra (Figure

Received: June 30, 2015
Published: August 10, 2015

DOI: 10.1021/jacs.5b06519
J. Am. Chem. Soc. 2015, 137, 10504−10507

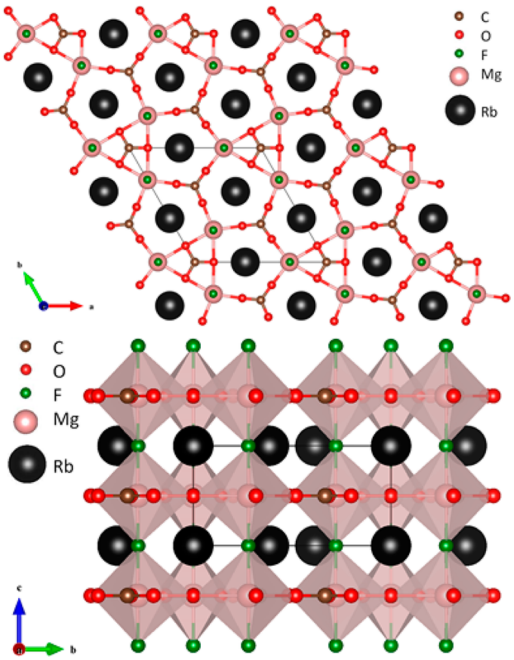

Figure 1. Ball-and-stick and polyhedral representation of $RbMgCO_3F$. In the top panel note that the Rb cations reside in the pentagonal "tunnels" created by the Mg polyhedra. In the bottom panel, note that the Mg polyhedra are connected by F atoms.

1). The Mg^{2+} cations are connected to carbonate groups in the *ab*-plane and a bridging fluoride along the *c*-direction. The Rb^+ cations are located in the cavities formed between the $Mg(CO_3)_3F_2$ groups. In connectivity terms, the materials may be described as $[Mg(CO_3)_{3/3}F_{2/2}]^-$ anions, with charge balance maintained by one Rb^+ cation. Each Mg^{2+} cation is bonded to four O-atoms and two F-atoms in a distorted octahedral coordination environment, with Mg−O distances of 1.9937(17)−2.1960(13) Å and an Mg−F distance of 1.9703(2) Å. The carbonate C−O bond distances range from 1.2724(9) to 1.2842(6) Å. The Rb^+ cation is surrounded by six O-atoms and three F-atoms, with Rb−O distances of 2.9262(8)−3.0991(8) Å and Rb−F distances of 3.0533(6)−3.0893(9) Å. Bond valence calculations resulted in values of 1.00, 2.09, and 3.99−4.12 for Rb^+, Mg^{2+}, and C^{4+}, respectively.

The coordination environment of the Mg^{2+} cation in $RbMgCO_3F$ is entirely different from that of the known alkaline-earth cations in the $ABCO_3F$ carbonate fluoride family (Figure 2). Mg^{2+} is found in a distorted octahedral coordination environment, MgO_4F_2, whereas other alkaline-earth cations are

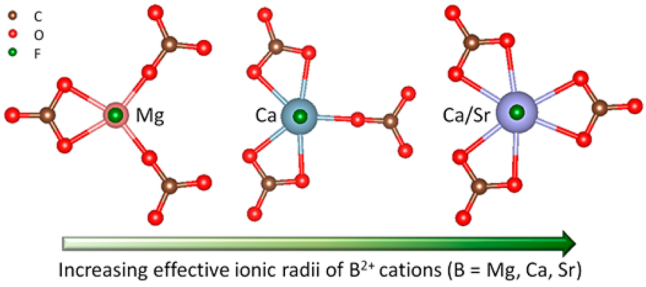

Figure 2. Different coordination denticities for B^{2+} cations (B = Mg, Ca, Sr) in $ABCO_3F$ materials (A = K, Rb, Cs). Note that, unique to Mg^{2+}, both monodentate and bidentate linkages are observed.

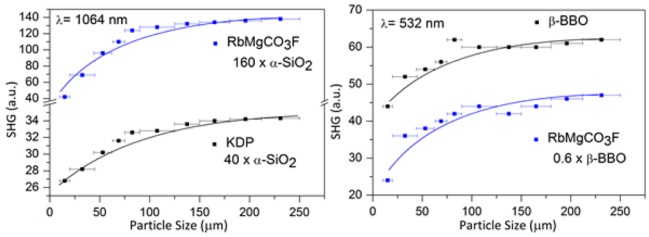

Figure 3. Powder second harmonic generation for $RbMgCO_3F$ at 1064 nm (left) and 532 nm (right). Curves are drawn to guide the eye and are not a fit to the data.

higher-fold coordinated, i.e., CaO_5F_2 (7-fold) in Rb(Cs)-$CaCO_3F$, CaO_6F_2 (8-fold) in $KCaCO_3F$, SrO_6F_2 (8-fold) in K(Rb)$SrCO_3F$, and BaO_6F_3 (9-fold) and BaO_6F_4 (10-fold) in $Cs_3Ba_4(CO_3)_3F_5$.[15] This evolution is attributed to the difference in the effective ionic radii; i.e., the radius of Mg^{2+} (0.72 Å, coordination number (C.N.) 6) is significantly smaller than those of other alkaline-earth cations, Ca^{2+} (1.06 Å, C.N. 7; and 1.12 Å, C.N. 8), Sr^{2+} (1.26 Å, C.N. 8), and Ba^{2+} (1.47 Å, C.N. 9; and 1.52 Å, C.N. 10).[17]

The coordination environment also produces a unique bonding pattern of $[Mg(CO_3)]_\infty$ layers. The layers are arranged in a pentagonal fashion in the (001) plane of $RbMgCO_3F$ that is not observed in the other members of the $ABCO_3F$ family. The Mg^{2+} cation is bonded to four O-atoms: two ligands, O(2), from one carbonate CO_3^{2-} group (bidentate) and the other two from two O-atoms, O(1), from separate (monodentate) CO_3^{2-} groups (Figure 2). This does not occur for the Ca^{2+} and Sr^{2+} cations in $ABCO_3F$ (A = K, Rb, Cs, B = Ca, Sr). In $[B(CO_3)]_\infty$ layers of $ABCO_3F$, the Ca^{2+} cation can be connected to either (i) five O-atoms, i.e., four from two bidentate CO_3^{2-} groups and one from a single CO_3^{2-} group ($RbCaCO_3F$ and $CsCaCO_3F$), or (ii) six O-atoms from three bidentate CO_3^{2-} units ($KCaCO_3F$).[15] For the Sr^{2+} cation, in $KSrCO_3F$ and $RbSrCO_3F$, the bonding pattern of $[Sr(CO_3)]_\infty$ is similar to that of $[Ca(CO_3)]_\infty$ (Figure 2).[15] This change in denticity can be distinguished using a formalism introduced in ref 18, which relies on the variance between the ionic radii of the A and B cations. Here we compute a cation radii variance of 0.21 $Å^2$ for $RbMgCO_3F$, which places it well beyond the range previously established to be compatible with aligned carbonate groups and three bidentate linkages (~0−0.07 $Å^2$, Figure 2, right).[18] Note that the former stability range was established for carbonate fluorides with a single formula unit per unit cell, $Z = 1$, whereas $RbMgCO_3F$ is more similar to $RbCaCO_3F$ and $CsCaCO_3F$, with $Z = 3$ and two bidentate linkages (variance > ~0.07, Figure 2, center). Here we report the first member within what is likely a family of compounds with $Z = 3$ and a *single* bidentate linkage of the B^{2+} cation in achiral nonpolar NCS carbonate fluorides (Figure 2, left). For borate fluorides, $BaMgBO_3F$ is also expected to exhibit a large cation variance that stabilizes single bidentate MgO_4F_2 units with $Z = 1$.[19]

Motivated by the unusual connectivity and the NCS space group $P\bar{6}2m$, we examined the SHG and piezoelectric properties. Powder SHG measurements using 1064 and 532 nm radiation revealed a SHG efficiency of approximately 160 × α-SiO_2 and 0.6 × β-BBO respectively, in the 45−63 μm particle size range. Additional SHG measurements, and particle size vs SHG efficiency, indicate the material exhibits type 1 phase-matching behavior (Figure 3). As such, $RbMgCO_3F$ falls into

DOI: 10.1021/jacs.5b06519
J. Am. Chem. Soc. 2015, 137, 10504−10507

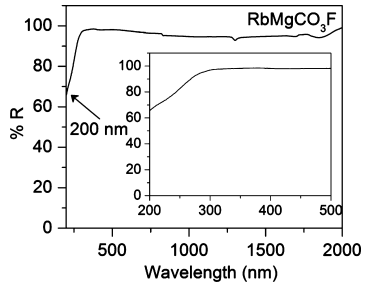

Figure 4. UV/vis diffuse reflectance data for $RbMgCO_3F$.

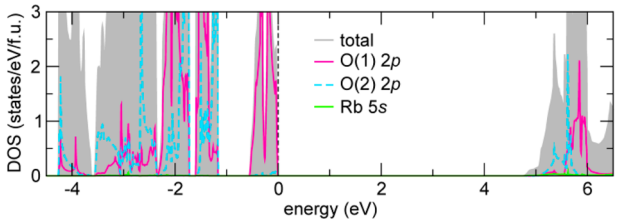

Figure 5. Electronic density of states (DOS) for $RbMgCO_3F$ decomposed by atomic site and orbital contributions. O(1) and O(2) correspond to Mg ligands which bond with monodentate and bidentate $[CO_3]^{2-}$ groups, respectively.

the class A category of SHG materials, as defined by Kurtz and Perry.[20] Converse piezoelectric measurement on $RbMgCO_3F$ was also performed, and a piezoelectric charge constant, d_{33}, of ~49 pm/V was determined.

The IR spectrum of $RbMgCO_3F$ revealed C−O, OCO, Mg−O, and Mg−F vibrations, consistent with previous reports.[21,22] The UV/vis diffuse reflectance and transmission spectra indicate that $RbMgCO_3F$ exhibits a wide transparency range from 2000 to 190 nm (Figures 4 and S4). Even at 200 nm, the reflectance is nearly 70%. This would indicate that $RbMgCO_3F$ is a promising DUV NLO material.

Figure 5 shows the atom-resolved DOS for $RbMgCO_3F$. The calculated band gap using PBEsol is 4.75 eV, which is ~2 eV smaller than the experimental value attributable to the systematic band gap underestimation of the semi-local functional. The calculated band gap of $RbMgCO_3F$ is much larger than that of $RbPbCO_3F$ calculated at the same theoretical level, consistent with our experiments.[15b] The smaller band gap for $RbPbCO_3F$ is mainly a consequence of the lone pair on Pb^{2+}.

The electronic structure of $RbMgCO_3F$ is also sharply different compared with that of $RbPbCO_3F$, in that the valence band maximum and conduction band minimum are dominated by O 2p and Rb 5s states, respectively, because Mg^{2+} is fully ionized and contributes states far from the Fermi energy. Upon atomic decomposition of the DOS, we find that the states at the valence band edge derive from the oxygen ligands O(1) bonded in a monodentate fashion with Mg, whereas the O(2) atoms with bidentate bonding are found lower in energy (approximately −2 to −1 eV). The fluorine 2p states, as expected, are found below those of both O-atoms within the energy range of −4 to −2.5 eV (not shown).

To understand in detail how the atomic structure provides for this electronic structure configuration and a SHG efficiency at 1064 nm, intermediate between $RbPbCO_3F$ (6.25 × KDP) and $RbSrCO_3F$ (3.33 × KDP), we compute the specific acentric mode displacements (SAMD).[1f] The calculated SAMD according to the previous definition[18] applied to carbonate

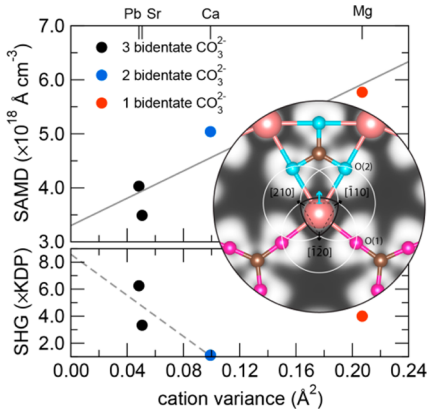

Figure 6. Effect of Rb and B cation variance on the carbonate linkage in $RbBCO_3F$ carbonate fluorides. The density of acentric displacements as parametrized in the SAMD value (see text) increases with the change in bonding of the B^{2+} cation with the carbonate group (top). The SHG response is anti-correlated with the cation variance for two and three bidentate carbonate groups (bottom), whereas the behavior of $RbMgCO_3F$ is found to be an outlier owing to reduced polarizable charge density in response to an electric field. The inset depicts charge-density contours of the ELF in the (001) plane about the Mg site with the static asymmetry greater than that found for the other compounds. The Reuleaux triangle construction is highlighted and, because of the bonding environment, should be puckered (no longer regular) along the vertical direction indicated by the light blue arrow.

fluorides is 5.77 × 10^{18} Å/cm^3 (Tables S5 and S6), which is larger than that of all $RbB^{2+}CO_3F$ (Figure 6). The mode consists mainly of oxygen and fluorine displacements within the *ab*-plane. As pointed out in our previous work, however, large SAMD does not necessitate a large NLO response, since three dipolar moments in $P\bar{6}2m$ align along the principal directions of a Reuleaux triangle located on the B^{2+} cation site and macroscopically cancel.[18] The moderate SHG intensity in $RbMgCO_3F$ is attributable to the increased SAMD in the achiral NCS material, which, although indicating a greater number of inversion symmetry lifting distortions in the structure, acts to constructively cancel an induced polarization arising from the oscillating electric field of an incident photon. The extent to which this occurs in $RbMgCO_3F$ is examined in the inset of Figure 6, which depicts the electron localization function (ELF) in the (001) plane.

As common to the NCS carbonate fluorides, we find clover-like electron density motifs for the carbonate units; however, those oxygen ligands forming a monodentate link to Mg^{2+} are more dimpled than those with the bidentate connectivity. As described in one of our earlier studies,[18] the B^{2+} cation is usually located at the center of a *regular* Reuleaux triangle formed by the nonbonding oxygen charge density. Interestingly, we find this triangle should be puckered in $RbMgCO_3F$, along the [120] direction (see light blue arrow in Figure 6), as a direct consequence of the single bidentate bonding geometry. The chelated geometry results in a greater static asymmetric distribution of charge. Nonetheless, the reduced electronic polarizability of Mg^{2+}, i.e., its position in the periodic table, above those of all the other B^{2+} cations found in $RbB^{2+}CO_3F$, *reduces* the electronic component of the SHG from the induced charge density oscillations under optical excitation.[23] $RbMgCO_3F$ then exhibits a response less than that of $RbPbCO_3F$, but greater than those of the Sr and Ca analogues, owing to the local asymmetry in the Mg−O bond lengths from

DOI: 10.1021/jacs.5b06519
J. Am. Chem. Soc. 2015, 137, 10504−10507

the denticity; i.e., the C−O(1) bond is 0.012 Å shorter than C−O(2).

Clearly, a large cation variance is key in stabilizing the pentagonal carbonate arrangement, and a sizable SHG is possible with a lower SAMD value. Using this crystal-chemistry understanding as an operational principle, we next examined computationally the isoelectronic alkali $CsMgCO_3F$ at the same level of theory. First, the cation variance is ∼0.28, greater than that for $RbMgCO_3F$, indicating that it is likely to form in the same structure. Next, because the band gap is sensitive to the chemical strain imposed by the AF layer on the BCO_3 planes, where the gap of $RbMgCO_3F$ (6.5 eV) > $RbCaCO_3F$ (6.2 eV) and $RbPbCO_3F$ (4.1 eV) < $CsPbCO_3F$ (4.15 eV), we anticipate a larger band gap (shorter cutoff wavelength) for $CsMgCO_3F$. To test this, we fully relaxed $CsMgCO_3F$ using the $P\bar{6}2m$ structure. As the DFT error for the semi-local functional is effectively constant across the family of carbonate fluorides,[12] we find the band gap of $CsMgCO_3F$ to be 5.01 eV, ∼0.25 eV larger than that of $RbMgCO_3F$. It also has a SAMD value of 3.71×10^{18} Å/cm^3, which should produce reasonable SHG intensities. Using the assumption that the error for the semi-local functional in DFT is constant across the family of carbonate fluorides, we predict that the experimental absorption edge in $CsMgCO_3F$ should be below 180 nm.

■ ASSOCIATED CONTENT

Supporting Information

The Supporting Information is available free of charge on the ACS Publications website at DOI: 10.1021/jacs.5b06519.

Experimental details, PXRD patterns, and X-ray crystallographic data (PDF, CIF)

■ AUTHOR INFORMATION

Corresponding Authors

*jrondinelli@northwestern.edu

*psh@uh.edu

Notes

The authors declare no competing financial interest.

■ ACKNOWLEDGMENTS

P.S.H. and T.T.T. thank the Welch Foundation (Grant E-1457) and NSF-DMR-1503573 for support. J.H. and J.M.R. thank NSF-DMR-1454688 for support. This work used the CARBON cluster at the Center for Nanoscale Materials at Argonne National Laboratory, supported by the U.S. DOE, Office of Science, Office of Basic Energy Sciences, under Contract No. DE-AC02-06CH11357. We also thank Prof. Kenneth R. Poeppelmeier and Dr. Shichao Wang (Northwestern University) for assistance in FTIR measurements.

■ REFERENCES

(1) (a) Xu, K.; Loiseau, P.; Aka, G. *J. Cryst. Growth* **2009**, *311*, 2508. (b) Yang, Y.; Pan, S.; Hou, X.; Wang, C.; Poeppelmeier, K. R.; Chen, Z.; Wu, H.; Zhou, Z. *J. Mater. Chem.* **2011**, *21*, 2890. (c) Wu, H.; Pan, S.; Poeppelmeier, K. R.; Li, H.; Jia, D.; Chen, Z.; Fan, X.; Yang, Y.; Rondinelli, J. M.; Luo, H. *J. Am. Chem. Soc.* **2011**, *133*, 7786. (d) Zhang, M.; Pan, S.; Yang, Z.; Wang, Y.; Su, X.; Yang, Y.; Huang, Z.; Han, S.; Poeppelmeier, K. R. *J. Mater. Chem. C* **2013**, *1*, 4740. (e) Wu, H.; Yu, H.; Pan, S.; Huang, Z.; Yang, X.; Su, K.; Poeppelmeier, K. R. *Angew. Chem., Int. Ed.* **2013**, *52*, 3406. (f) Wu, H.; Yu, H.; Yang, Z.; Hou, X.; Su, X.; Pan, S.; Poeppelmeier, K. R.; Rondinelli, J. M. *J. Am. Chem. Soc.* **2013**, *135*, 4215. (g) Yu, H.; Wu, W.; Pan, S.; Yang, Z.; Hou, X.; Su, X.; Jing, Q.; Poeppelmeier, K. R.; Rondinelli, J. M. *J. Am. Chem. Soc.* **2014**, *136*, 1264. (h) Yan, X.; Luo, S.; Yao, J.; He, R.; Yue, Y.; Chen, C.; Lin, Z. *Inorg. Chem.* **2014**, *53*, 1952. (i) Zhao, S.; Gong, P.; Bai, L.; Xu, X.; Zhang, S.; Sun, Z.; Lin, Z.; Hong, M.; Chen, C.; Luo, J. *Nat. Commun.* **2014**, *5*, 4019. (j) Yu, H.; Wu, H.; Pan, S.; Yang, Z.; Hou, X.; Su, X.; Jing, Q.; Poeppelmeier, K. R.; Rondinelli, J. M. *J. Am. Chem. Soc.* **2014**, *136*, 1264.

(2) (a) Savage, N. *Nat. Photonics* **2007**, *1*, 83. (b) Cyranoski, D. *Nature (London, U. K.)* **2009**, *457*, 953. (c) Yao, W.; He, R.; Wang, X.; Lin, Z.; Chen, C. *Adv. Opt. Mater.* **2014**, *2*, 411.

(3) Chen, C. T.; Wang, G. I.; Wang, X. Y.; Xu, Z. Y. *Appl. Phys. B: Lasers Opt.* **2009**, *97*, 9.

(4) (a) Ye, N.; Tang, D. Y. *J. Cryst. Growth* **2006**, *293*, 233. (b) McMillen, C. D.; Kolis, J. W. *J. Cryst. Growth* **2008**, *310*, 2033. (c) Chen, C. T.; Wang, G. L.; Wang, X. Y.; Xu, Z. Y. *Appl. Phys. B: Lasers Opt.* **2009**, *97*, 9.

(5) Chen, C. T.; Wu, Y. C.; Jiang, A. D.; Wu, B. C.; You, G. M.; Li, R. K.; Lin, S. J. *J. Opt. Soc. Am. B* **1989**, *6*, 616.

(6) Wu, Y. C.; Sasaki, T.; Nakai, N.; Yokotani, A.; Tang, H. G.; Chen, C. T. *Appl. Phys. Lett.* **1993**, *62*, 2614.

(7) Chen, C.; Sasaki, T.; Li, R. K.; Wu, Y.; Lin, Z.; Mori, Y.; Hu, Z.; Wang, J.; Uda, S.; Yoshimura, M.; Kaneda, Y. *Nonlinear Optical Borate Crystals: Principles and Applications*; Wiley: Weinheim, 2012.

(8) Eimerl, D.; Davis, L.; Velsko, S.; Graham, E. K. *J. Appl. Phys.* **1987**, *62*, 1968.

(9) (a) Halasyamani, P. S.; Poeppelmeier, K. R. *Chem. Mater.* **1998**, *10*, 2753. (b) Ra, H.-S.; Ok, K. M.; Halasyamani, P. S. *J. Am. Chem. Soc.* **2003**, *125*, 7764. (c) Sun, C.-F.; Hu, C.-L.; Xu, X.; Ling, J.-B.; Hu, T.; Kong, F.; Long, X.-F.; Mao, J.-G. *J. Am. Chem. Soc.* **2009**, *131*, 9486. (d) Donakowski, M. D.; Gautier, R.; Yeon, J.; Moore, D. T.; Nino, J. C.; Halasyamani, P. S.; Poeppelmeier, K. R. *J. Am. Chem. Soc.* **2012**, *134*, 7679.

(10) (a) Yang, B. P.; Hu, C.-L.; Xu, X.; Sun, C.-F.; Zhang, J.-H.; Mao, J.-G. *Chem. Mater.* **2010**, *22*, 1545. (b) Nguyen, S. D.; Yeon, J.; Kim, S.-H.; Halasyamani, P. S. *J. Am. Chem. Soc.* **2011**, *133*, 12422. (c) Cao, X.-L.; Hu, C.-L.; Xu, X.; Kong, F.; Mao, J.-G. *Chem. Commun.* **2013**, *49*, 9965. (d) Huang, C.; Hu, C.-L.; Xu, X.; Yang, B.-P.; Mao, J.-G. *Dalton Trans.* **2013**, *42*, 7051. (e) Yang, B.-P.; Hu, C.-L.; Xu, X.; Huang, C.; Mao, J.-G. *Inorg. Chem.* **2013**, *52*, 5378. (f) Xu, X.; Yang, B.-P.; Huang, C.; Mao, J.-G. *Inorg. Chem.* **2014**, *53*, 1756. (g) Jo, H.; Kim, Y. H.; Lee, D. W.; Ok, K. M. *Dalton Trans.* **2014**, *43*, 11752. (h) Kim, Y. H.; Lee, D. W.; Ok, K. M. *Inorg. Chem.* **2014**, *53*, 5240. (i) Kim, Y. H.; Lee, D. W.; Ok, K. M. *Inorg. Chem.* **2014**, *53*, 1250.

(11) (a) Chung, I.; Kanatzidis, M. G. *Chem. Mater.* **2014**, *26*, 849. (b) Brant, J. A.; Clark, D. J.; Kim, Y. S.; Jang, J. I.; Zhang, J.-H.; Aitken, J. A. *Chem. Mater.* **2014**, *26*, 3045. (c) Rosmus, K. A.; Brant, J. A.; Wisneski, S. D.; Clark, D. J.; Kim, Y. S.; Jang, J. I.; Brunetta, C. D.; Zhang, J.-H.; Srnec, M. N.; Aitken, J. A. *Inorg. Chem.* **2014**, *53*, 7809.

(12) Kang, L.; Luo, S.; Huang, H.; Ye, N.; Lin, Z.; Qin, J.; Chen, C. *J. Phys. Chem. C* **2013**, *117*, 25684.

(13) Grice, J. D.; Maisonneuve, V.; Leblanc, M. *Chem. Rev.* **2007**, *107*, 114.

(14) (a) Chen, C. T.; Yu, W. C.; Lin, R. K. *Chin. Phys. Lett.* **1985**, *2*, 389. (b) Chen, C. T. *Materials for Nonlinear Optics* **1991**, *455*, 360. (c) Chen, C. T. *Laser Science and Technology: An International Handbook*; Harwood Academic Press, 1993; Vol. *15*.

(15) (a) Zou, G.; Ye, N.; Huang, H.; Lin, X. *J. Am. Chem. Soc.* **2011**, *133*, 20001. (b) Tran, T. T.; Halasyamani, P. S.; Rondinelli, J. M. *Inorg. Chem.* **2014**, *53*, 6241.

(16) Luo, M.; Ye, N.; Zou, G.; Lin, C.; Cheng, W. *Chem. Mater.* **2013**, *25*, 3147.

(17) Shannon, R. D. *Acta Crystallogr., Sect. A* **1976**, *32*, 751.

(18) Cammarata, A.; Zhang, W.; Halasyamani, P. S.; Rondinelli, J. M. *Chem. Mater.* **2014**, *26*, 5773.

(19) Li, R. K.; Chen, P. *Inorg. Chem.* **2010**, *49*, 1561.

(20) Abrahams, S. C.; Kurtz, S. K.; Jamieson, P. B. *Phys. Rev.* **1968**, *172*, 551.

(21) Huang, C. K.; Kerr, P. F. *Am. Mineral.* **1960**, *45*, 311.

(22) Lesiecki, M. L.; Nibler, J. W. *J. Chem. Phys.* **1976**, *64*, 871.

(23) Levine, B. F. *Phys. Rev. B* **1973**, *7*, 2600.

DOI: 10.1021/jacs.5b06519
J. Am. Chem. Soc. 2015, 137, 10504−10507